Available online at www.sciencedirect.com
SCIENCE DIRECT®
International Journal of Solids and Structures 42 (2005) 3185–3205
INTERNATIONAL JOURNAL OF SOLIDS and STRUCTURES
www.elsevier.com/locate/ijsolstr

Dynamic analysis of a cracked magnetoelectroelastic medium under antiplane mechanical and inplane electric and magnetic impacts

Xian-Fang Li *

Institute of Mechanics and Sensor Technology, School of Civil Engineering and Architecture, Central South University, Changsha, Hunan 410083, PR China
College of Mathematics and Computer Science, Hunan Normal University, Changsha, Hunan 410081, PR China

Received 6 October 2004
Available online 30 November 2004

Abstract

The transient analysis of a magnetoelectroelastic medium containing a crack is made under antiplane mechanical and inplane electric and magnetic impacts. The crack is assumed to penetrate through the solid along the poling direction. By using the Fourier and Laplace transforms, the associated mixed boundary value problem is reduced to a Fredholm integral equation of the second kind, which is solved numerically. By means of a numerical inversion of the Laplace transform, dynamic field intensity factors are obtained in the time domain. Numerical results are presented graphically to show the effects of the material properties and applied electric and magnetic impacts on the dynamic intensity factors of COD and stress, and dynamic energy density factors. The results indicate that except for the intensity factors of electric displacement and magnetic induction, other field intensity factors exhibit apparent transient feature. Moreover, they depend strongly on mechanical input as well as electric and magnetic impacts.

Keywords: Magnetoelectroelastic medium; Crack; Transient response; Dynamic field intensity factors; Energy density factor

1. Introduction

Due to the intrinsic coupling between mechanical and electric behaviors in piezoelectric materials, piezoelectric materials have been widely used in microelectromechanical systems as sensors, actuators, and

* Address: Institute of Mechanics and Sensor Technology, School of Civil Engineering and Architecture, Central South University, Changsha, Hunan 410083, PR China. Tel.: +86 73 1887 2667; fax: +86 73 1887 2260.
E-mail address: xfli@post.com

0020-7683/$ - see front matter © 2004 Elsevier Ltd. All rights reserved.
doi:10.1016/j.ijsolstr.2004.10.020

transducers, etc. Furthermore, in a class of piezoelectric/piezomagnetic composites consisting of piezoelectric and piezomagnetic phases, not only the interaction of mechanical and electric fields but also the interactions of mechanical and magnetic, and electric and magnetic fields are present, and owing to this characteristic, which can interchange the internal energies stored in mechanical, electric, and magnetic forms, piezoelectric/piezomagnetic composites are potential candidates for fabricating a new generation of smart or intelligent structures. For such piezoelectric/piezomagnetic composites, effective material properties have been predicted according to the viewpoint of micromechanics via various approaches by researchers including Li and Dunn (1998), Huang et al. (1998), Aboudi (2001), among others. In particular, a surprising magnetoelectric coupling between electric and magnetic fields under low frequency can take place, and it is, however, not present in arbitrary single-phase piezoelectric or piezomagnetic material. Moreover, the magnetoelectric coefficients depend strongly upon the volume fraction of each constituent as well as the configuration of inclusions such as bulk composites, fibrous reinforced composites, and layered composites (Nan, 1994; Benveniste, 1995; Li, 2000). In addition, within the framework of the theory of linear magnetoelectroelasticity, a general magnetoelectroelastic solution has been put forward for a transversely isotropic magnetoelectroelastic solid by Wang and Shen (2002), and for a spherically isotropic magnetoelectroelastic solid by Wang and Zhong (2003), respectively.

On the other hand, for piezoelectric/piezomagnetic composites, a main disadvantage is that they are very susceptible to fracture because of their brittleness. Owing to various causes, cracks or flaws are inevitably present in such magnetoelectroelastic materials. For a magnetoelectroelastic material with cracks subjected to applied magnetoelectromechanical loading, magnetoelectroelastic field concentration occurs near cracks, which probably rises high enough to cause crack advance, and finally leads to serious degradation of the performance of magnetoelectroelastic materials. To understand the failure mechanism of magnetoelectroelastic materials, the analysis of elastic, electric and magnetic behaviors in a cracked magnetoelectroelastic solid subjected to applied magnetoelectroelastic loading is prerequisite. Along this line, Green's functions for anisotropic magnetoelectroelastic solids with an elliptical cavity or a crack have been obtained (Liu et al., 2001). Furthermore, Wang and Mai (2003, 2004) investigated the problems involving an antiplane shear crack and a plane crack in a magnetoelectroelastic medium where the crack surface is assumed to be impermeable to electric and magnetic field, similar to the electric boundary condition at the crack surface used in treating crack problems of piezoelectric materials (Pak, 1990). A similar antiplane impermeable crack problem was also treated by Spyropoulos et al. (2003), who assumed magnetoelectric coupling coefficient of a magnetoelectroelastic solid to vanish. In contrast to the above analysis, using the permeable electric and magnetic boundary conditions at the crack surface instead of the impermeable boundary conditions, Gao et al. (2003a,b,c) studied the distribution of the magnetoelectroelastic field disturbed by a single crack and collinear cracks in a magnetoelectroelastic solid, and by an interfacial crack between two dissimilar magnetoelectroelastic media, respectively. The influence of magnetic field and electric field on crack growth in particular for crack initiation angle has been investigated under various boundary conditions including so-called mode-I, mode-II, and mixed mode crack by Sih and Chen (2003), Sih and Song (2003), and Sih et al. (2003).

The above-mentioned works are mainly related to static problems. However, under various time-dependent loadings the study of dynamic mechanical, electrical and magnetic behaviors in a magnetoelectroelastic material with a crack is of great significance. To the best of the author's knowledge, so far the dynamic response problem of a cracked magnetoelectroelastic material has not been considered.

This paper is concerned with the transient response of magnetoelectroelastic field of a magnetoelectroelastic solid with a crack under sudden magnetoelectroelastic impact loading. The crack is assumed to be penetrate through the medium along the poling direction. The problem is reduced to a Fredholm integral equation of the second kind by using the Fourier and Laplace transforms. Solving the resulting equation numerically and performing a numerical inversion of the Laplace transform, dynamic field intensity factors are obtained in the time domain. The results are presented graphically and the effects of the material prop-

erties on the dynamic COD intensity factors, dynamic stress intensity factors, and dynamic energy density factors are examined.

2. Statement of the problem

For a linearly magnetoelectroelastic solid subjected to external electric and/or magnetic fields, not only the electric displacement and magnetic induction can be caused, but also the mechanical deformation of the magnetoelectroelastic medium can be induced owing to the coupling of elastic, electric and magnetic behaviors. Conversely, an applied mechanical loading can produce electric field and magnetic field, in addition to mechanical deformation. The relationship of the interactions of mechanical, electric, and magnetic fields in magnetoelectroelastic materials can be described by the following full-couplied constitutive equations

$$\sigma = \mathbf{C}\mathbf{s} - \mathbf{e}\mathbf{E} - \mathbf{h}\mathbf{H}, \tag{1}$$

$$\mathbf{D} = \mathbf{e}\mathbf{s} + \varepsilon\mathbf{E} + \mathbf{d}\mathbf{H}, \tag{2}$$

$$\mathbf{B} = \mathbf{h}\mathbf{s} + \mathbf{d}\mathbf{E} + \mu\mathbf{H}, \tag{3}$$

where σ, $\mathbf{D}$, and $\mathbf{B}$ are the stress tensor, electric displacement vector, and magnetic induction vector, respectively; $\mathbf{s}$, $\mathbf{E}$, and $\mathbf{H}$ are the strain tensor, electric field vector, and magnetic field vector, respectively; $\mathbf{C}$, ε, and μ are the elastic modulus tensor, dielectric constant tensor, and magnetic permittivity tensor, respectively; $\mathbf{e}$, $\mathbf{h}$, and $\mathbf{d}$ are the piezoelectric, piezomagnetic, and magnetoelectric coefficient tensors. It is noted that the above constitutive equations are limited to the case of low frequency, implying that electric and magnetic fields can be treated as static case.

Consider a transversely isotropic magnetoelectroelastic solid with a through Griffith crack lying at $|x| \leqslant a$, $y = 0$, $-\infty < z < \infty$, as shown in Fig. 1. Here Cartesian coordinates x, y, z are the principal axes of the material symmetry while the z-axis is the symmetry axis of the magnetoelectroelastic solid. Thus we have the material properties as follows

$$\mathbf{C} = \begin{bmatrix} c_{11} & c_{12} & c_{13} & 0 & 0 & 0 \\ c_{12} & c_{11} & c_{13} & 0 & 0 & 0 \\ c_{13} & c_{13} & c_{33} & 0 & 0 & 0 \\ 0 & 0 & 0 & 2c_{44} & 0 & 0 \\ 0 & 0 & 0 & 0 & 2c_{44} & 0 \\ 0 & 0 & 0 & 0 & 0 & c_{11} - c_{12} \end{bmatrix}, \tag{4}$$

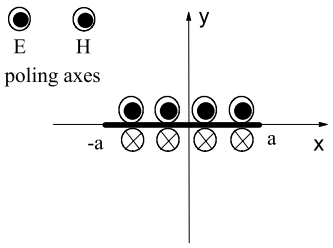

Fig. 1. Schematic of an antiplane shear crack in a magnetoelectroelastic material along with associated coordinates.

$$\mathbf{e}=\begin{bmatrix} 0 & 0 & e_{31} \\ 0 & 0 & e_{31} \\ 0 & 0 & e_{33} \\ 0 & e_{15} & 0 \\ e_{15} & 0 & 0 \\ 0 & 0 & 0 \end{bmatrix}, \quad \mathbf{h}=\begin{bmatrix} 0 & 0 & h_{31} \\ 0 & 0 & h_{31} \\ 0 & 0 & h_{33} \\ 0 & h_{15} & 0 \\ h_{15} & 0 & 0 \\ 0 & 0 & 0 \end{bmatrix}, \tag{5}$$

$$\varepsilon=\begin{bmatrix} \varepsilon_{11} & 0 & 0 \\ 0 & \varepsilon_{11} & 0 \\ 0 & 0 & \varepsilon_{33} \end{bmatrix}, \quad \mu=\begin{bmatrix} \mu_{11} & 0 & 0 \\ 0 & \mu_{11} & 0 \\ 0 & 0 & \mu_{33} \end{bmatrix}, \quad d=\begin{bmatrix} d_{11} & 0 & 0 \\ 0 & d_{11} & 0 \\ 0 & 0 & d_{33} \end{bmatrix}, \tag{6}$$

which contain 17 constants, including five elastic constants, two dielectric constants, two magnetic primitivities, three piezoelectric constants, three piezomagnetic constants, and two magnetoelectric constants.

In what follows our attention is focused on the case where a magnetoelectroelastic solid is subjected to sudden antiplane mechanical impact and inplane electric and magnetic impacts with respect to the *xoy*-plane. In this case we have

$$u_1 = u_2 = 0, \quad E_3 = 0, \quad B_3 = 0,$$

and there are only nonvanishing out-of-plane elastic displacement $u_3 = w(x, y, t)$, inplane electric potential $\phi(x, y, t)$, and inplane magnetic potential $\varphi(x, y, t)$. Under such circumstances, the stress, electric displacement, and magnetic induction are related to w, ϕ, and φ by the following constitutive equations

$$\sigma_{xz} = c_{44}w_{,x} + e_{15}\phi_{,x} + h_{15}\varphi_{,x}, \quad \sigma_{yz} = c_{44}w_{,y} + e_{15}\phi_{,y} + h_{15}\varphi_{,y}, \tag{7}$$

$$D_x = e_{15}w_{,x} - \varepsilon_{11}\phi_{,x} - d_{11}\varphi_{,x}, \quad D_y = e_{15}w_{,y} - \varepsilon_{11}\phi_{,y} - d_{11}\varphi_{,y}, \tag{8}$$

$$B_x = h_{15}w_{,x} - d_{11}\phi_{,x} - \mu_{11}\varphi_{,x}, \quad B_y = h_{15}w_{,y} - d_{11}\phi_{,y} - \mu_{11}\varphi_{,y}, \tag{9}$$

where the comma denotes partial differentiation with respect to the suffix space variable. Here, six independent nonvanishing material constants are involved. In particular, if neglecting the piezomagnetic and magnetoelectric coefficients, the constitutive equations for a single-phase piezoelectric ceramic in a state of antiplane deformation can be recovered from the above, while if neglecting the piezoelectric and magnetoelectric coefficients, the constitutive equations for a single-phase piezomagnetic material in a state of antiplane deformation can be recovered from the above. Furthermore, if imposing the piezoelectric, piezomagnetic and magnetoelectric coefficients to vanish, the constitutive equations for a purely elastic medium in a state of antiplane deformation can be revived.

Based on the above constitutive equations, it follows from the equation of motion and the Maxwell equations that $w(x, y, t)$, $\phi(x, y, t)$ and $\varphi(x, y, t)$ satisfy the basic governing differential equations for dynamics problems of a magnetoelectroelastic solid in a state of antiplane deformation

$$c_{44}\nabla^2 w + e_{15}\nabla^2\phi + h_{15}\nabla^2\varphi = \rho\frac{\partial^2 w}{\partial t^2}, \tag{10}$$

$$e_{15}\nabla^2 w - \varepsilon_{11}\nabla^2\phi - d_{11}\nabla^2\varphi = 0, \tag{11}$$

$$h_{15}\nabla^2 w - d_{11}\nabla^2\phi - \mu_{11}\nabla^2\varphi = 0, \tag{12}$$

where ρ is the mass density of the magnetoelectroelastic medium, and ∇^2 represents the two-dimensional Laplacian operator. Here body forces, free charges, and current densities have been neglected.

To obtain a solution of the above-stated dynamic problem involving a crack, appropriate boundary conditions at the crack surfaces must be furnished. Of much interest from the viewpoint of fracture mechanics is the singular crack-tip field disturbed by a crack subjected to applied impact loadings. Furthermore, owing to symmetry of the problem it is sufficient to consider the corresponding problem in the upper half-plane $y \geqslant 0$, so in the following we confine our attention to this region. Consequently, the mechanical, electric, and magnetic boundary conditions at the crack surfaces can be stated below

$$\sigma_{yz}(x,0,t) = -\sigma_0(x)f(t), \quad |x| < a, \ t > 0, \tag{13}$$

$$D_y(x,0,t) = -D_0(x)f(t), \quad |x| < a, \ t > 0, \tag{14}$$

$$B_y(x,0,t) = -B_0(x)f(t), \quad |x| < a, \ t > 0, \tag{15}$$

where $f(t)$ is a prescribed function in time t, $f(t) = 0$ as $t \leqslant 0$, and $\sigma_0(x)$, $D_0(x)$, and $B_0(x)$ are prescribed functions.

3. Solution of the problem

It is seen from Eqs. (10)–(12) that w, ϕ, and φ are coupled. To decouple them, a simple approach is to introduce two new functions ζ and η such that

$$\phi = \zeta - \frac{d_{11}}{\varepsilon_{11}}\eta + \frac{e_{15}\mu_{11} - h_{15}d_{11}}{\varepsilon_{11}\mu_{11} - d_{11}^2}w, \tag{16}$$

$$\varphi = \eta - \frac{d_{11}}{\mu_{11}}\zeta + \frac{h_{15}\varepsilon_{11} - e_{15}d_{11}}{\varepsilon_{11}\mu_{11} - d_{11}^2}w. \tag{17}$$

Thus, Eqs. (10)–(12) then become

$$\nabla^2 w = \frac{1}{c_s^2}\frac{\partial^2 w}{\partial t^2}, \tag{18}$$

$$\nabla^2 \zeta = 0, \tag{19}$$

$$\nabla^2 \eta = 0, \tag{20}$$

with

$$c_s = \sqrt{\frac{c_m}{\rho}}, \quad c_m = c_{44} + \frac{\varepsilon_{11}h_{15}^2 + \mu_{11}e_{15}^2 - 2h_{15}e_{15}d_{11}}{\varepsilon_{11}\mu_{11} - d_{11}^2}, \tag{21}$$

$c_s = \sqrt{c_m/\rho}$ being the shear wave velocity of a magnetoelectroelastic material. Obviously, the shear wave velocity c_s is related to all the material constants appearing in the constitutive equations (7)–(9).

In order to obtain a desired electroelastic field, for convenience it is necessary to impose that a magnetoelectroelastic medium is initially at rest. Namely, a magnetoelectroelastic material is subjected to the vanishing initial conditions:

$$w|_{t=0} = 0, \quad \frac{\partial w}{\partial t}|_{t=0} = 0, \tag{22}$$

$$\phi|_{t=0} = 0, \quad \frac{\partial \phi}{\partial t}|_{t=0} = 0, \tag{23}$$

$$\varphi|_{t=0} = 0, \quad \frac{\partial \varphi}{\partial t}|_{t=0} = 0. \tag{24}$$

Additionally, a solution should be sought under the regularity conditions. In other words, all the elastic, electric and magnetic quantities will vanish as $y \to \infty$. Accordingly, performing the Laplace transform with respect to t and the Fourier cosine transform with respect to x to both sides of Eq. (18) yields

$$\frac{\mathrm{d}^2 \hat{w}^*}{\mathrm{d}y^2} - \left(\xi^2 + \frac{p^2}{c_s^2}\right)\hat{w}^* = 0, \tag{25}$$

where a quantity with the asterisk denotes the Laplace transform with respect to t of this quantity, defined by

$$f^*(p) = \int_0^\infty f(t)\,\mathrm{e}^{-pt}\,\mathrm{d}t, \tag{26}$$

and the circumflex over a quantity stands for the Fourier cosine transform with respect to x, defined by

$$\hat{f}(\xi) = \int_0^\infty f(x)\cos(\xi x)\,\mathrm{d}x, \tag{27}$$

p and ξ being the parameters of the Laplace and Fourier transforms, respectively. Solving the ordinary differential equation (25) under the regularity conditions, we obtain a formal solution in the transform-domain. From this solution, making use of the inverse Fourier cosine transform leads to the out-of-plane displacement in the Laplace transform domain, expressed by

$$w^* = \int_0^\infty A(\xi, p)\exp(-\alpha y)\cos(\xi x)\,\mathrm{d}\xi \tag{28}$$

where

$$\alpha = \sqrt{\xi^2 + \frac{p^2}{c_s^2}}, \tag{29}$$

and $A(\xi,p)$ is unknown to be determined through appropriate boundary conditions.

Using the same routine, we can get similar expressions for the introduced functions ζ and η from Eqs. (19) and (20), respectively. Namely,

$$\zeta^* = \int_0^\infty M(\xi)\exp(-\xi y)\cos(\xi x)\,\mathrm{d}\xi, \tag{30}$$

$$\eta^* = \int_0^\infty N(\xi)\exp(-\xi y)\cos(\xi x)\,\mathrm{d}\xi, \tag{31}$$

where unknown $M(\xi)$ and $N(\xi)$ can be determined through appropriate boundary conditions. Once $A(\xi,p)$, $M(\xi)$ and $N(\xi)$ are determined, w, ζ and η can be obtained in the Laplace transform domain, and further in the physical space only by performing the inverse Laplace transform. In the following we utilize given boundary conditions to look for the unknown $A(\xi,p)$, $M(\xi)$ and $N(\xi)$.

To this end, one can apply the Laplace transform to Eqs. (7)–(9), together with the vanishing initial conditions. Especially, one can get

$$\sigma_{yz}^* = c_{44} w_{,y}^* + e_{15}\phi_{,y}^* + h_{15}\varphi_{,y}^*, \tag{32}$$

$$D_y^* = e_{15} w_{,y}^* - \varepsilon_{11} \phi_{,y}^* - d_{11} \varphi_{,y}^*, \tag{33}$$

$$B_y^* = h_{15} w_{,y}^* - d_{11} \phi_{,y}^* - \mu_{11} \varphi_{,y}^*, \tag{34}$$

Hence, substituting (28), (30) and (31) into the Laplace transform of (16) and (17), then into (32)–(34) results in the expressions for the components of the stress, electric displacement and magnetic induction in the Laplace transform domain in terms of $A(\xi, p)$, $M(\xi)$ and $N(\xi)$, i.e.

$$\sigma_{yz}^* = -c_m \int_0^\infty \alpha A(\xi) \exp(-\alpha y) \cos(\xi x)\, d\xi - \int_0^\infty \xi \left[\left(e_{15} - \frac{h_{15} d_{11}}{\mu_{11}} \right) M(\xi) + \left(h_{15} - \frac{e_{15} d_{11}}{\varepsilon_{11}} \right) N(\xi) \right] \exp(-\xi y) \cos(\xi x)\, d\xi, \tag{35}$$

$$D_y^* = \frac{\varepsilon_{11}\mu_{11} - d_{11}^2}{\mu_{11}} \int_0^\infty \xi M(\xi) \exp(-\xi y) \cos(\xi x)\, d\xi, \tag{36}$$

$$B_y^* = \frac{\varepsilon_{11}\mu_{11} - d_{11}^2}{\varepsilon_{11}} \int_0^\infty \xi N(\xi) \exp(-\xi y) \cos(\xi x)\, d\xi, \tag{37}$$

for $y \geqslant 0$.

Now, application of the Laplace transform to the boundary conditions (13)–(15) yields

$$\sigma_{yz}^*(x, 0, p) = -\sigma_0(x) f^*(p), \quad |x| < a, \tag{38}$$

$$D_y^*(x, 0, p) = -D_0(x) f^*(p), \quad |x| < a, \tag{39}$$

$$B_y^*(x, 0, p) = -B_0(x) f^*(p), \quad |x| < a, \tag{40}$$

In the above results we use the expressions (35)–(37) for σ_{yz}^*, D_y^*, and B_y^*, and, after some algebra, get

$$\int_0^\infty \alpha A(\xi, p) \cos(\xi x)\, d\xi = \frac{1}{c_m} \tau_0(x) f^*(p), \quad |x| < a, \tag{41}$$

$$\int_0^\infty \xi M(\xi) \cos(\xi x)\, d\xi = -\frac{\mu_{11}}{\varepsilon_{11}\mu_{11} - d_{11}^2} D_0(x) f^*(p), \quad |x| < a, \tag{42}$$

$$\int_0^\infty \xi N(\xi) \cos(\xi x)\, d\xi = -\frac{\varepsilon_{11}}{\varepsilon_{11}\mu_{11} - d_{11}^2} B_0(x) f^*(p), \quad |x| < a, \tag{43}$$

with

$$\tau_0(x) = \sigma_0(x) + \frac{e_{15}\mu_{11} - h_{15} d_{11}}{\varepsilon_{11}\mu_{11} - d_{11}^2} D_0(x) + \frac{h_{15}\varepsilon_{11} - e_{15} d_{11}}{\varepsilon_{11}\mu_{11} - d_{11}^2} B_0(x). \tag{44}$$

On the other hand, from the following boundary conditions

$$w(x, 0, t) = 0, \quad |x| > a, \ t > 0, \tag{45}$$

$$\phi(x, 0, t) = 0, \quad |x| > a, \ t > 0, \tag{46}$$

$$\varphi(x, 0, t) = 0, \quad |x| > a, \ t > 0, \tag{47}$$

derived from the symmetry of the considered problem, in connection with (28), (30) and (31) one can derive

$$\int_0^\infty A(\xi,p)\cos(\xi x)\,\mathrm{d}\xi = 0, \quad |x| > a, \tag{48}$$

$$\int_0^\infty M(\xi)\cos(\xi x)\,\mathrm{d}\xi = 0, \quad |x| > a, \tag{49}$$

$$\int_0^\infty N(\xi)\cos(\xi x)\,\mathrm{d}\xi = 0, \quad |x| > a. \tag{50}$$

Hence, we get three decoupled systems of simultaneous dual integral equations for $A(\xi,p)$, $M(\xi)$, and $N(\xi)$. Clearly, in addition to the functions of the right-hand side, the dual integral equations for $M(\xi)$ are the same in form as those for $N(\xi)$, and they are a special case of the dual integral equations for $A(\xi,p)$ with the requirement $\alpha = \xi$. Therefore, in what follows for convenience we only deal with the dual integral equations for $A(\xi,p)$. The solution of such dual integral equations can be derived by using the techniques, outlined in Chen and Sih (1977). That is, if the unknown function $A(\xi,p)$ is represented as the following integral

$$A(\xi,p) = \int_0^a \chi(s,p) J_0(s\xi)\,\mathrm{d}s, \tag{51}$$

where $J_0(\cdot)$ is the Bessel function of the first kind of order zero, and $\chi(s,p)$ is a new auxiliary function, it is easily shown that due to the following identity

$$\int_0^\infty J_0(s\xi)\cos(\xi x)\,\mathrm{d}\xi = 0, \quad x > s. \tag{52}$$

Eq. (48) is automatically fulfilled when substituting (51) into (48). In addition, inserting (51) into (41), after some manipulations we get a Fredholm integral equation of the second kind for the introduced auxiliary function $\chi(x,p)$:

$$\chi(x,p) + x\int_0^a K(x,s,p)\chi(s,p)\,\mathrm{d}s = \frac{2x}{\pi c_\mathrm{m}} f^*(p)\int_0^x \frac{\tau_0(s)}{\sqrt{x^2-s^2}}\,\mathrm{d}s, \quad 0 \leqslant x < a, \tag{53}$$

with the kernel $K(x,s,p)$, given by

$$K(x,s,p) = \int_0^\infty (\alpha - \xi) J_0(s\xi) J_0(x\xi)\,\mathrm{d}\xi. \tag{54}$$

In deriving the above Fredholm integral equation, we have employed the known results

$$J_0(x\xi) = \frac{2}{\pi}\int_0^x \frac{\cos(s\xi)}{\sqrt{x^2-s^2}}\,\mathrm{d}s, \tag{55}$$

and

$$\int_0^\infty \xi J_0(s\xi) J_0(x\xi)\,\mathrm{d}\xi = \frac{1}{x}\delta(x-s), \tag{56}$$

where $\delta(\cdot)$ denotes the Dirac delta function.

Owing to the complicated form of the kernel in Eq. (53), it seems unlikely that a closed-form solution can be derived for general cases. A numerical solution of the resulting Fredholm integral equation, however, is readily determined by a standard scheme. Prior to the presentation of its numerical solution, let us consider the special case where $\alpha = \xi$. It can be understood as the limiting case of $p \to 0$, which, in the physical space,

corresponds to a dynamic solution when $t \to \infty$, i.e. the corresponding static solution. In fact, a comparison of (41) and (42) indicates that the solution of dual integral equations for $M(\xi)$ can be obtained by setting $\alpha = \xi$ in the above-obtained solution. Accordingly, when $\alpha = \xi$, a closed-form solution can readily obtained to be

$$\chi(x,p) = \frac{2x}{\pi c_m} f^*(p) \int_0^x \frac{\tau_0(s)}{\sqrt{x^2 - s^2}}\,\mathrm{d}s, \quad 0 \leqslant x < a. \tag{57}$$

Especially, when $\tau_0(s) = \tau_0$, the above solution reduces to

$$\chi(x,p) = \frac{\tau_0}{c_m} x f^*(p). \tag{58}$$

In the following we appeal to a numerical method for solving the resulting Fredholm integral equation (53). For the purpose of numerical computation, the variables are normalized by the crack half-length a, i.e.

$$\bar{x} = \frac{x}{a}, \quad \bar{s} = \frac{s}{a}, \quad \bar{\chi}(\bar{x},p) = \frac{c_m \chi(x,p)}{a}, \tag{59}$$

and Eq. (53) is then rewritten as

$$\bar{\chi}(\bar{x},p) + \bar{x} \int_0^1 K(\bar{x},\bar{s},p)\bar{\chi}(\bar{s},p)\,\mathrm{d}\bar{s} = \frac{2\bar{x}}{\pi} f^*(p) \int_0^{\bar{x}} \frac{\tau_0(a\bar{s})}{\sqrt{\bar{x}^2 - \bar{s}^2}}\,\mathrm{d}\bar{s}, \quad 0 \leqslant \bar{x} < 1, \tag{60}$$

where

$$K(\bar{x},\bar{s},p) = \int_0^\infty \left[\sqrt{\xi^2 + (ap/c_s)^2} - \xi\right] J_0(\bar{s}\xi) J_0(\bar{x}\xi)\,\mathrm{d}\xi. \tag{61}$$

Taking into account the fact that the function $\sqrt{\xi^2 + (ap/c_s)^2} - \xi$ in the integrand of the kernel behaves as $O(1/\xi)$ for large ξ, this leads to very slow convergence of this integral. To accelerate convergence of this integral, denoting

$$R(\xi,p) = \sqrt{\xi^2 + (ap/c_s)^2} - \xi - \frac{(ap/c_s)^2 \xi}{2[\xi^2 + (ap/c_s)^2]} \tag{62}$$

we find

$$R(\xi,p) \simeq \mathrm{O}\left(\frac{1}{\xi^3}\right), \quad \text{for large } \xi. \tag{63}$$

Therefore, utilizing the following result

$$\int_0^\infty \frac{\xi}{\xi^2 + (ap/c_s)^2} J_0(\bar{s}\xi) J_0(\bar{x}\xi) d\xi = I_0(\bar{x}ap/c_s) K_0(\bar{s}ap/c_s), \quad 0 < \bar{x} \leqslant \bar{s}. \tag{64}$$

$I_0(\cdot)$ and $K_0(\cdot)$ being the modified zero order Bessel functions of the first and second kind, respectively, one can rewrite the kernel in Eq. (60) as

$$K(\bar{x},\bar{s},p) = \frac{(ap/c_s)^2}{2} I_0(\bar{x}ap/c_s) K_0(\bar{s}ap/c_s) + \int_0^\infty R(\xi,p) J_0(\bar{s}\xi) J_0(\bar{x}\xi)\,\mathrm{d}\xi, \quad 0 < \bar{x} \leqslant \bar{s}. \tag{65}$$

It is obvious that the integral in the second term at the right-hand side in the above equation can be then evaluated by a truncated integral due to its rapid convergence.

4. Field intensity factors

In this section, we determine the transient response of the crack-tip field under external stimulus. From the viewpoint of fracture mechanics, of much interest is the field intensity factors, which are commonly used to characterize the crack-tip field and chosen as significant fracture parameters.

With the above results in hand, it is easily found that the remaining is to seek w, together with $w_{,y}$. Knowledge of w, in conjunction with ζ and η, allows us to get all desired dynamic field intensity factors and crack-tip field. To obtain an asymptotic expression for crack opening displacement w^* in the Laplace transform domain behind the crack tip, putting (51) into (28) it is sufficient to evaluate the following integral

$$w^*(x,0,p)=\int_0^\infty\int_0^a \chi(s,p)J_0(s\xi)\cos(\xi x)\,\mathrm{d}s\,\mathrm{d}\xi=\int_x^a \frac{\chi(s,p)}{\sqrt{s^2-x^2}}\,\mathrm{d}s,\quad x<a, \tag{66}$$

so one can get

$$w^*(x,0,p)=\frac{\chi(a,p)}{a}\sqrt{a^2-x^2}+\mathrm{O}(r),\quad r=a-x\ll a, \tag{67}$$

with the COD intensity factor

$$K^*_{\mathrm{COD}}=\lim_{x\to a^-}\sqrt{\frac{\pi}{2(a-x)}}w(x,0)=\frac{\bar{\gamma}(1,p)}{c_{\mathrm{m}}}\sqrt{\pi a}. \tag{68}$$

Furthermore, the strain component $w^*_{,y}$ in the Laplace transform domain ahead of the crack tip can be obtained by evaluating the following integral

$$w^*_{,y}(x,0,p)=-\int_0^\infty\int_0^a \alpha\chi(s,p)J_0(s\xi)\cos(\xi x)\,\mathrm{d}s\,\mathrm{d}\xi,\quad x>a, \tag{69}$$

after some calculations, the asymptotic expression for $w^*_{,y}(x,0,p)$ near the crack tip is follows

$$w^*_{,y}(x,0,p)=\frac{x\chi(a,p)}{a\sqrt{x^2-a^2}}+\mathrm{O}(1). \tag{70}$$

It is easily shown that the strain intensity factor K^{γ} coincides with the above-obtained COD intensity factor K_{COD}.

Once K^*_{COD} is determined in the Laplace transform domain, K_{COD} can be derived by using the inverse Laplace transform technique. As pointed out in the above, it is unlikely that a closed-form expression for the solution of the Fredholm integral equation of the second kind (60) can be obtained because of the complexity of the kernel. Therefore, an explicit expression for COD in the physical space cannot be given in closed form. Instead, in what follows we employ a numerical inversion technique of the Laplace transform to get the COD intensity factor in the time domain.

On the other hand, based on the results given in the preceding section, for $D_0(x)=D_0$, $B_0(x)=B_0$, we get explicit analytic solutions of the dual integral equations for $M(\xi)$ and $N(\xi)$, respectively, as

$$M(\xi)=-\frac{\mu_{11}aJ_1(a\xi)}{(\varepsilon_{11}\mu_{11}-d_{11}^2)\xi}D_0f^*(p), \tag{71}$$

$$N(\xi)=-\frac{\varepsilon_{11}aJ_1(a\xi)}{(\varepsilon_{11}\mu_{11}-d_{11}^2)\xi}B_0f^*(p). \tag{72}$$

Furthermore, upon substitution of the above results into (30), (31), by performing the inverse Laplace transform, explicit expressions for ζ and η can be arrived at as follows

$$\zeta = -\frac{\mu_{11}}{\varepsilon_{11}\mu_{11} - d_{11}^2}\left[\sqrt{l_2^2 - x^2} - y\right] D_0 f(t), \tag{73}$$

$$\eta = -\frac{\varepsilon_{11}}{\varepsilon_{11}\mu_{11} - d_{11}^2}\left[\sqrt{l_2^2 - x^2} - y\right] B_0 f(t). \tag{74}$$

Moreover, from (36) and (37) one further get electric displacement and magnetic induction in the entire upper-plane as

$$D_y(x, y, t) = D_0\left[\frac{l_2\sqrt{l_2^2 - a^2}}{l_2^2 - l_1^2} - 1\right] f(t), \tag{75}$$

$$B_y(x, y, t) = B_0\left[\frac{l_2\sqrt{l_2^2 - a^2}}{l_2^2 - l_1^2} - 1\right] f(t). \tag{76}$$

Here we have used some known results, given in Fabrikant (2003), for example

$$\int_0^\infty \frac{1}{\xi} J_1(a\xi)\exp(-\xi y)\cos(\xi x)\,\mathrm{d}\xi = \frac{1}{a}\left[\sqrt{l_2^2 - x^2} - y\right], \tag{77}$$

$$\int_0^\infty J_1(a\xi)\exp(-\xi y)\cos(\xi x)\,\mathrm{d}\xi = \frac{1}{a} - \frac{l_2}{a}\frac{\sqrt{l_2^2 - a^2}}{l_2^2 - l_1^2}, \tag{78}$$

with

$$l_1 = \frac{1}{2}\left[\sqrt{(a+x)^2 + y^2} - \sqrt{(a-x)^2 + y^2}\right], \tag{79}$$

$$l_2 = \frac{1}{2}\left[\sqrt{(a+x)^2 + y^2} + \sqrt{(a-x)^2 + y^2}\right]. \tag{80}$$

In particular, at the crack line, we have

$$D_y(x, 0, t) = D_0\left[\frac{x}{\sqrt{x^2 - a^2}} - 1\right] f(t), \tag{81}$$

$$B_y(x, 0, t) = B_0\left[\frac{x}{\sqrt{x^2 - a^2}} - 1\right] f(t). \tag{82}$$

Obviously, electric displacement and magnetic induction near the crack tips have a usual square-root singularity, but not transient response, which are only proportional to prescribed time function $f(t)$. This conclusion is in agreement with the premise of the adopted theoretical model limited to the case of low frequency. With the above these results in hand, other intensity factors in the physical space can be determined by the following relations

$$K^\sigma = c_\mathrm{m} K_\mathrm{COD} + \frac{d_{11}h_{15} - \mu_{11}e_{15}}{\varepsilon_{11}\mu_{11} - d_{11}^2} K^D + \frac{d_{11}e_{15} - \varepsilon_{11}h_{15}}{\varepsilon_{11}\mu_{11} - d_{11}^2} K^B, \tag{83}$$

$$K^E = \frac{d_{11}h_{15} - \mu_{11}e_{15}}{\varepsilon_{11}\mu_{11} - d_{11}^2}K_{\mathrm{COD}} + \frac{\mu_{11}}{\varepsilon_{11}\mu_{11} - d_{11}^2}K^D - \frac{d_{11}}{\varepsilon_{11}\mu_{11} - d_{11}^2}K^B, \tag{84}$$

$$K^H = \frac{d_{11}e_{15} - \varepsilon_{11}h_{15}}{\varepsilon_{11}\mu_{11} - d_{11}^2}K_{\mathrm{COD}} - \frac{d_{11}}{\varepsilon_{11}\mu_{11} - d_{11}^2}K^D + \frac{\varepsilon_{11}}{\varepsilon_{11}\mu_{11} - d_{11}^2}K^B, \tag{85}$$

with

$$K^D = \sqrt{\pi a}D_0 f(t), \quad K^B = \sqrt{\pi a}B_0 f(t). \tag{86}$$

Based on the viewpoint of energy, energy density factor around the crack tip is an important fracture parameter in predicting crack propagation in piezoelectric/piezomagnetic composites (Song and Sih, 2003; Sih and Chen, 2003; Sih and Song, 2003; Sih et al., 2003; Spyropoulos et al., 2003). Using the above results, after some manipulations we can get dynamic energy density factors for the situation under consideration as

$$S(t) = \tfrac{1}{2}\Big[c_{44}(K_{\mathrm{COD}})^2 + \varepsilon_{11}(K^E)^2 + \mu_{11}(K^H)^2 + 2d_{11}K^E K^H\Big]. \tag{87}$$

5. Numerical results

In this section, the effects of the material properties on the dynamic normalized field intensity factors are examined for a cracked piezoelectric/piezomagnetic composite made of the piezoelectric $BaTiO_3$ material as the inclusions and piezomagnetic (magnetostrictive) $CeFe_2O_4$ material as the matrix. The relevant material properties of the piezoelectric phase $BaTiO_3$ and the piezomagnetic phase $CeFe_2O_4$ are listed in Table 1. For convenience, the material constants of the magnetoelectroelastic $BaTiO_3$–$CeFe_2O_4$ composite are assumed to obey the mixture rule (Song and Sih, 2003), i.e.

$$\kappa^c = \kappa^i V_{\mathrm{f}} + \kappa^m(1 - V_{\mathrm{f}}), \tag{88}$$

where κ with the superscripts c, i, m denotes the corresponding constants of c_{44}, ε_{11}, μ_{11}, e_{15}, h_{15} of the composite, inclusion, and matrix, respectively, and V_{f} is the volume fraction of the piezoelectric phase $BaTiO_3$. Due to the absence of magnetoelectric coupling coefficient in a single-phase piezoelectric or piezomagnetic material, the magnetoelectric constant d_{11} existing only in the piezoelectric/piezomagnetic composite as a significant new feature cannot be determined by the above mixture rule. Therefore, based on the analysis of micromechanics, this coefficient is chosen as $d_{11} = 5.2 \times 10^{-12}$ (N s/VC) for a fibrous reinforced composite, and $d_{11} = -3.6 \times 10^{-8}$ (Ns/VC) for a laminated composite when $V_{\mathrm{f}} = 0.5$ (Li, 2000), respectively.

In the following, we take time impact function as the Heaviside unit step function, i.e. $f(t) = H(t)$, and $\sigma_0(x) = \sigma_0$, $D_0(x) = D_0$, $B_0(x) = B_0$. In this case, from the results obtained in the preceding section, it is easily seen that the intensity factors of the electric displacement and magnetic induction do not vary with time, while the COD intensity factor, in connection with other intensity factors, vary with time. In other words, the latter dynamic field intensity factors exhibit a transient characteristic. Moreover, K_{COD} depends on the material properties owing to (68), and so do other dynamic field intensity factors since they are represented in terms of K_{COD}.

Table 1
The relevant material properties

	c_{44} (GPa)	ε_{11} (C^2/Nm^2)	μ_{11} (Ns^2/C^2)	e_{15} (C/m^2)	h_{15} (N/A m)	d_{11} (N s/VC)
$BaTiO_3$	43	11.2×10^{-9}	5×10^{-6}	11.6	0	0
$CoFe_2O_4$	45.3	80×10^{-12}	-590×10^{-6}	0	550	0

To obtain the dynamic intensity factors in the physical space, the inverse Laplace transform must be performed. Because of the difficulty to derive an explicit analytic solution, a numerical approach for carrying out the inversion of the Laplace transform proposed by Stehfest (1970) is invoked to obtain dynamic field intensity factors in the time domain. That is, once $\bar{\chi}(1,p)$ in the Laplace transform domain is determined numerically, its inversion $g(1,t)$ can be determined by the following scheme

$$g(1,t) \simeq \frac{\ln(2)}{t} \sum_{n=1}^{2L} V_n \bar{\chi}\left[1, \frac{n\ln(2)}{t}\right], \tag{89}$$

with

$$V_n = (-1)^{n+L} \sum_{m=[(n+1)/2]}^{\min(n,L)} \frac{m^N (2m)!}{(L-m)!m!(m-1)!(n-m)!(2m-n)!}, \tag{90}$$

where $[(n+1)/2]$ is the integer part of the real number $(n+1)/2$. This method not only has reasonable accuracy for a fairly wide range of Laplace transforms (Davies and Martin, 1979), and but also is very easy and simple, as compared to other numerical inversions such as Miller and Guy (1966). In (89) only one parameter L is involved, which is suggested by Stehfest (1970) to be taken as lower integers, while more than two parameters are involved in other methods for an inversion of the Laplace transform.

Fig. 2 shows the response of normalized dynamic COD intensity factor $c_{44}K_{\mathrm{COD}}/\sigma_0\sqrt{\pi a}$ versus normalized time $c_s t/a$ for the piezoelectric $BaTiO_3$ material, the piezomagnetic $CoFe_2O_4$ material, and piezoelectric/piezomagnetic $BaTiO_3$–$CoFe_2O_4$ composite under purely mechanical impact. It is found that the response curve as well as the overshoot of dynamic COD intensity factor of the $BaTiO_3$–$CoFe_2O_4$ composite lie in the intermediate between the counterparts of single $BaTiO_3$ or $CoFe_2O_4$ material, implying that the response characteristic of the $BaTiO_3$–$CoFe_2O_4$ composite differs from each constituent. However, there are not evident difference for a fibrous composite and a laminated composite. This is easily understood since only mechanical impact is applied. In addition, for comparison, numerical results obtained by the

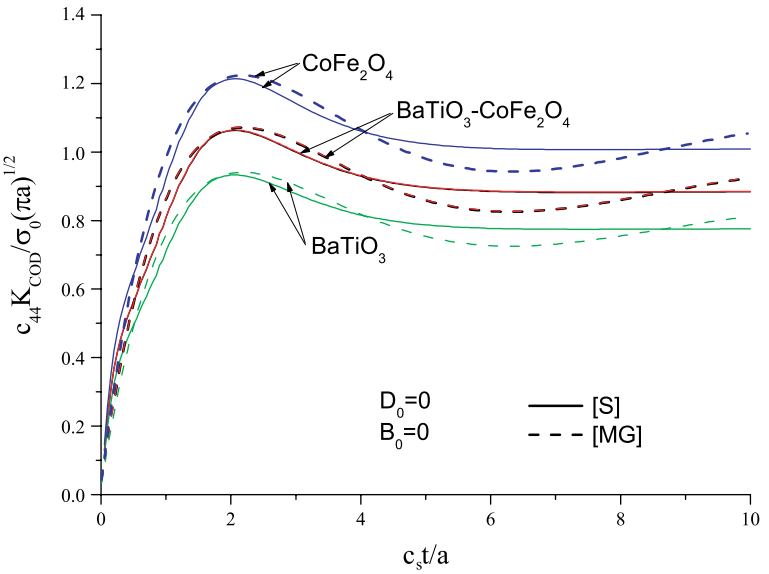

Fig. 2. Comparison of the variations of normalized dynamic COD intensity factor vs normalized time via Stehfest's and Miller and Guy's methods.

Miller and Guy's numerical inversion of Laplace transform are also plotted with dashed lines in Fig. 2. Obviously, the results derived by the above two methods are in satisfactory agreement. Moreover, we find that the overshoots of all response curves occur at the same normalized time about $c_s t/a = 2.1$. This is to say that the practical time arriving at the peak will be delayed when c_s becomes small for different materials.

In the following, the normalized dynamic intensity factors of COD and stress for the $BaTiO_3$–$CoFe_2O_4$ composite are depicted under combined applied impacts. When subjected to external electric stimulus and mechanical impact, the response curves of the dynamic COD intensity factor with applied magnetic induction $B_0/\sigma_0 = 0.2 \times 10^{-6}$ m/A are shown in Figs. 3 and 4, respectively. From Figs. 3 and 4 one can find that the transient response is similar to that of the dynamic stress intensity factor for a cracked elastic medium. That is, after applied impact is suddenly exerted, response curves rise abruptly, arriving at an overshoot, then decrease gradually, and finally approach to the corresponding static value. Furthermore, it is seen that a positive electric impact increases the COD intensity factors, while a negative one decreases the COD intensity factors. In particular, from Fig. 4 in the presence of magnetic loading, $B_0/\sigma_0 = 0.2 \times 10^{-6}$ m/A, the responses of fibrous and laminated composites with a crack exist apparent difference, indicating the influence of the magnetoelectric coefficient on the dynamic COD intensity factor. This discrepancy will disappear in the absence of applied magnetic loading in Fig. 3, since in this case the response of a cracked fibrous composite coincides with that of a cracked laminated composite. As a by-product, it is observed that when time becomes large enough, the static COD intensity factor can be derived, inferring that a positive electric loading promotes crack growth, and a negative one hinders crack growth for fixed applied magnetic loading. Note that here the COD intensity factor is chosen as a fracture criterion in magnetoelectroelastic materials, just as in piezoelectric materials, and its superiority over the stress intensity factor as a fracture criterion has been elucidated for piezoelectric materials (Li and Lee, 2004a,b).

The variations of the normalized dynamic COD intensity factors under the action of external magnetic and mechanical impact loadings with $D_0/\sigma_0 = 0.25 \times 10^{-9}$ C/N are illustrated in Figs. 5 and 6, respectively. By inspection, the trends in Figs. 5 and 6 are similar to those in Figs. 3 and 4. However, for fixed electric loading, a positive magnetic loading decreases the COD intensity factor, while a negative one increases the

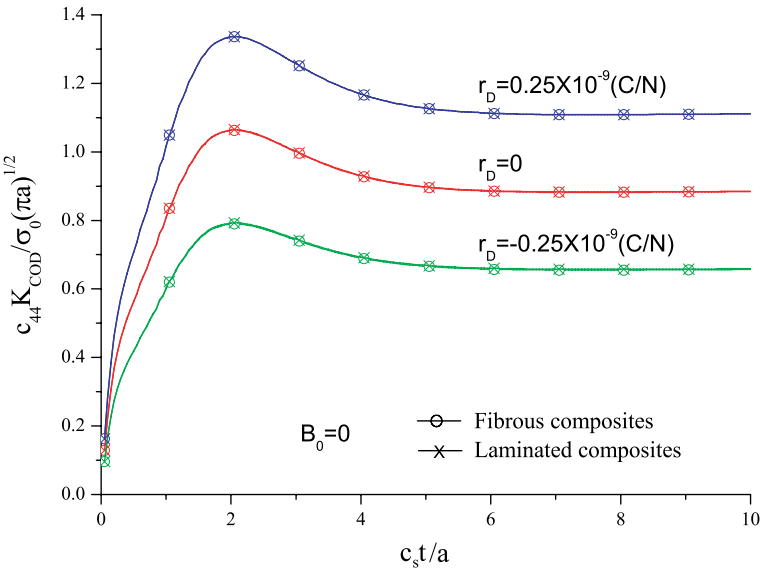

Fig. 3. Transient response of the normalized dynamic COD intensity factor under different electric and mechanical impacts in the absence of magnetic loading.

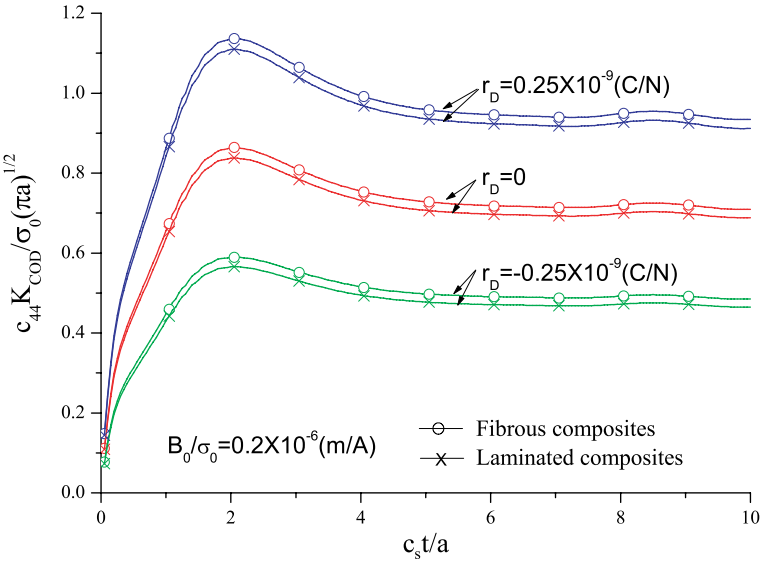

Fig. 4. Transient response of the normalized dynamic COD intensity factor under different electric and mechanical impacts in the presence of magnetic loading.

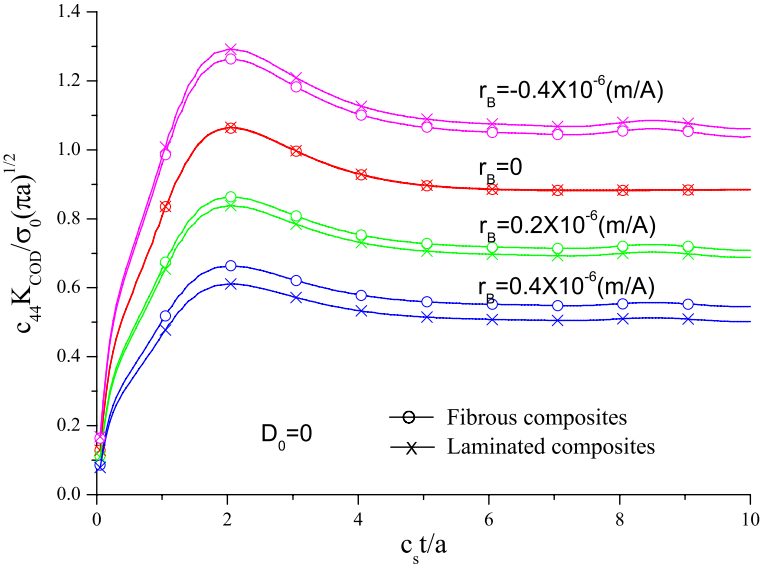

Fig. 5. Transient response of the normalized dynamic COD intensity factor under different magnetic and mechanical impacts in the absence of electric loading.

COD intensity factor, which is completely opposite to the effect of applied electric loading on the COD intensity factor. This is attributed to a negative piezomagnetic constant and a positive piezoelectric constant. So, a positive magnetic loading impedes crack propagation and a negative one aids crack propagation. Moreover, the effect of the magnetoelectric coefficient on dynamic COD intensity factor is very evident in the presence of applied magnetic loading, even for $D_0 = 0$.

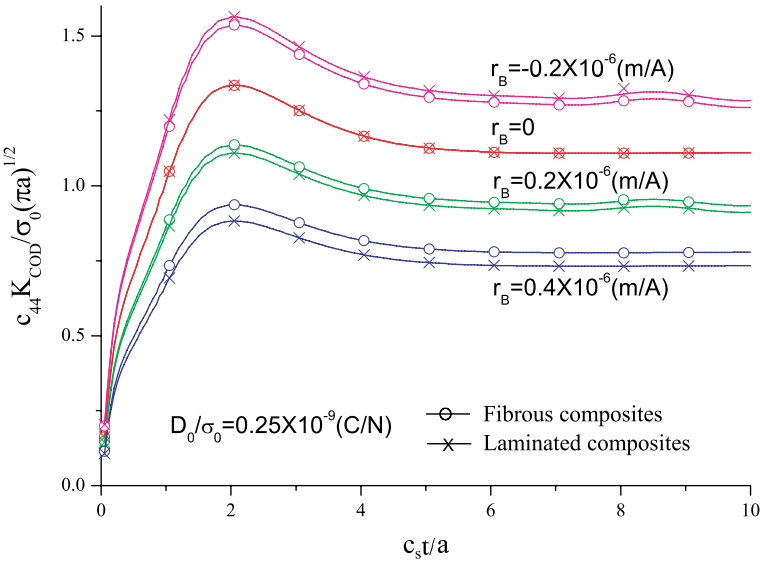

Fig. 6. Transient response of the normalized dynamic COD intensity factor under different magnetic and mechanical impacts in the presence of electric loading.

Figs. 7–9 are devoted to the effects of electric and magnetic impacts on dynamic stress intensity factors. The variation of dynamic stress intensity factors for fibrous and laminated composites subjected to sudden different electric and mechanical impacts is depicted in Fig. 7. It has been shown in Wang and Mai (2004) that stress intensity factor in the static case is independent of applied electric and magnetic loadings. This is not true for the corresponding dynamic case. Clearly, it is seen from Figs. 7–9 that at the early stage of the action of applied impact loadings, dynamic stress intensity factors are dramatically affected by electric and

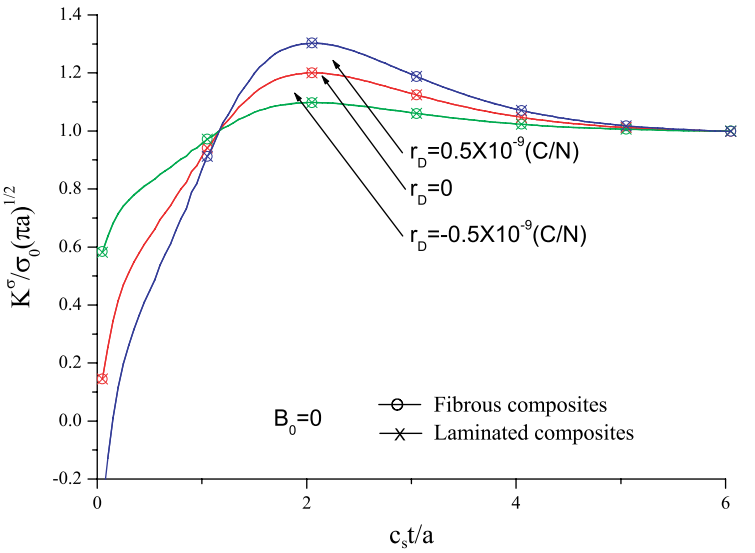

Fig. 7. Variation of the normalized dynamic stress intensity factor with the normalized time when no magnetic loading is applied.

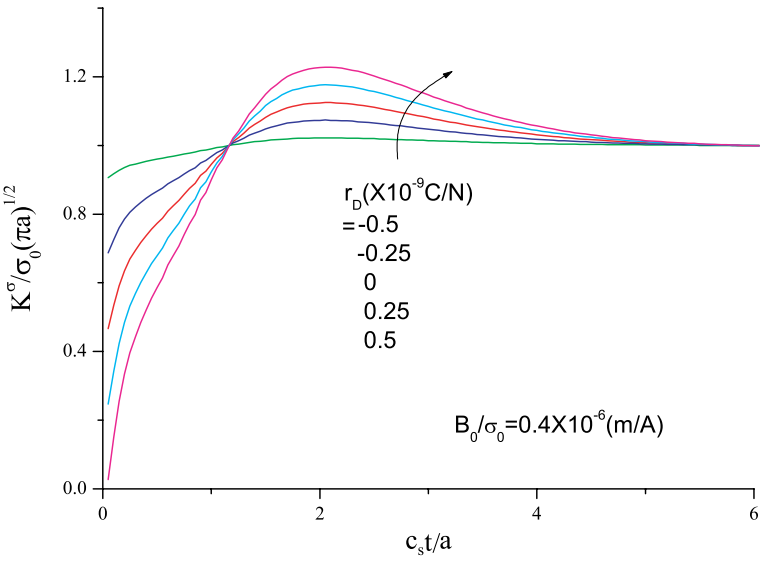

Fig. 8. Influence of electric impact on dynamic stress intensity factor.

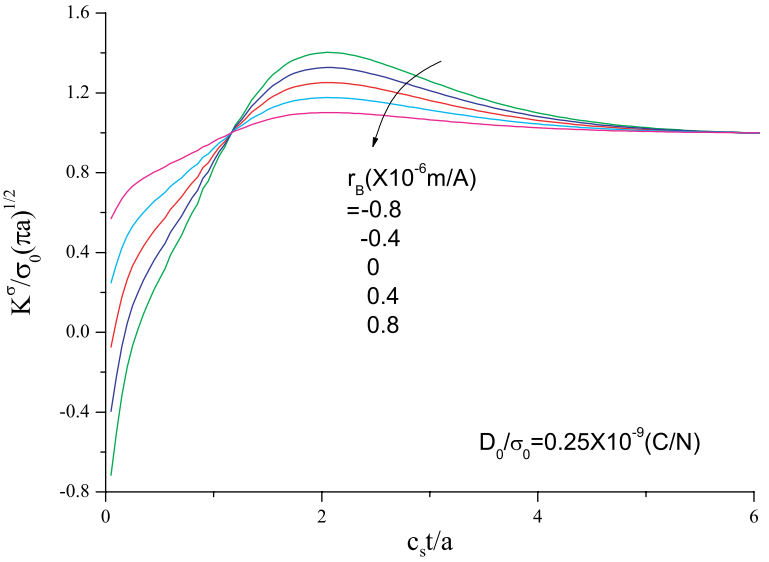

Fig. 9. Influence of magnetic impact on dynamic stress intensity factor.

magnetic impact loadings. Moreover, the effects of electric and magnetic loadings on the peak of dynamic stress intensity factor are different. Or rather, the overshoot of dynamic stress intensity factor rises with the increase of electric loading from Fig. 8, or with the decrease of magnetic loading from Fig. 9. And when time becomes large enough, the effects of electric and magnetic loadings disappear, and dynamic stress intensity factor tends to the corresponding static value, related to neither electric loading nor magnetic loading. It is further observed that the response of dynamic stress intensity factor has little relationship with the magnetoelectric coefficient.

Another interesting investigation is the variation of dynamic energy density factor around the crack tip with time. With the results obtained above, dynamic energy density factor is easily evaluated through (87). Some numerical results are presented in the following figures. Figs. 10 and 11 show respectively the dynamic energy density factor normalized by the corresponding static value at the absence of and in the presence of applied magnetic loading for the $BaTiO_3$–$CoFe_2O_4$ composite. It is seen that there is significant

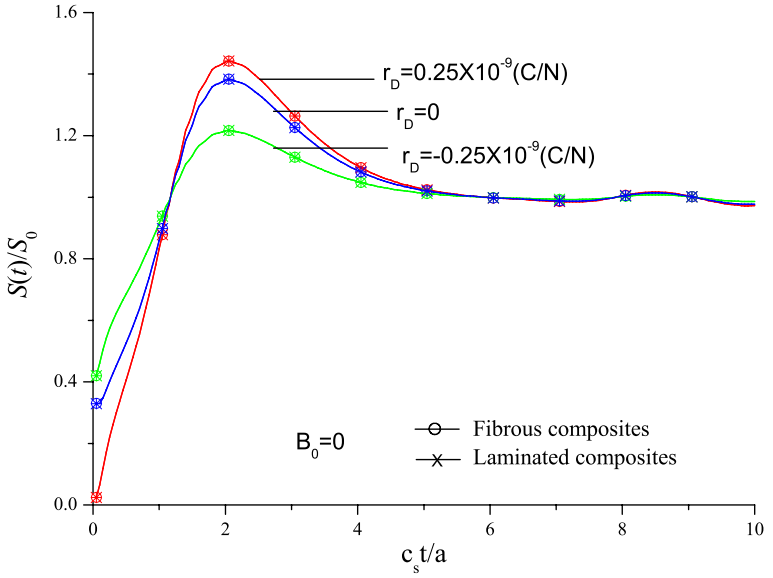

Fig. 10. Dynamic energy density factor vs normalized time for $B_0 = 0$.

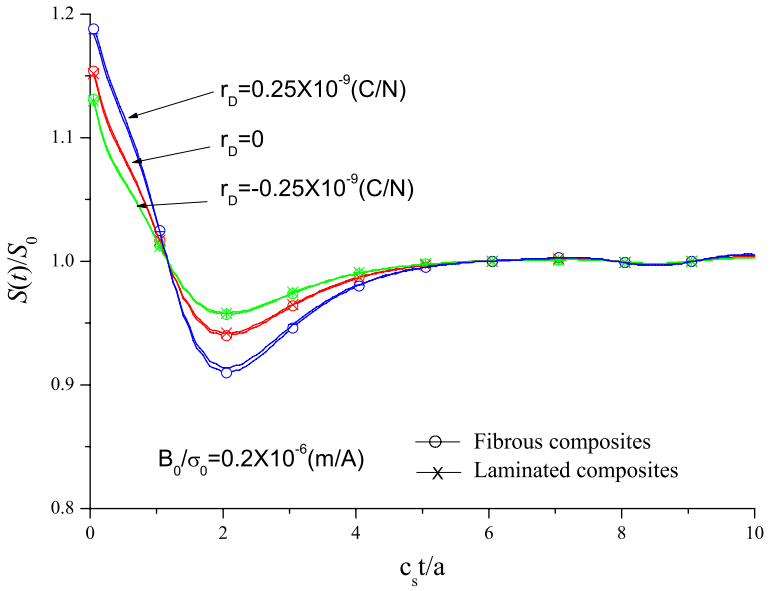

Fig. 11. Dynamic energy density factor vs normalized time for $B_0/\sigma_0 = 0.2 \times 10^{-6}$ m/A.

difference between the dynamic normalized energy density factors corresponding to $B_0 = 0$ and $B_0/\sigma_0 = 0,0.2 \times 10^{-6}$ m/A, implying that applied magnetic loading has an important contribution of dynamic energy density factor. In contrast, for applied electric loading, Figs. 12 and 13 illustrate the influence of applied electric loading on dynamic energy factor, which indicates that the effect is very small for the cases of $D_0/\sigma_0 = 0.25 \times 10^{-9}$ C/N.

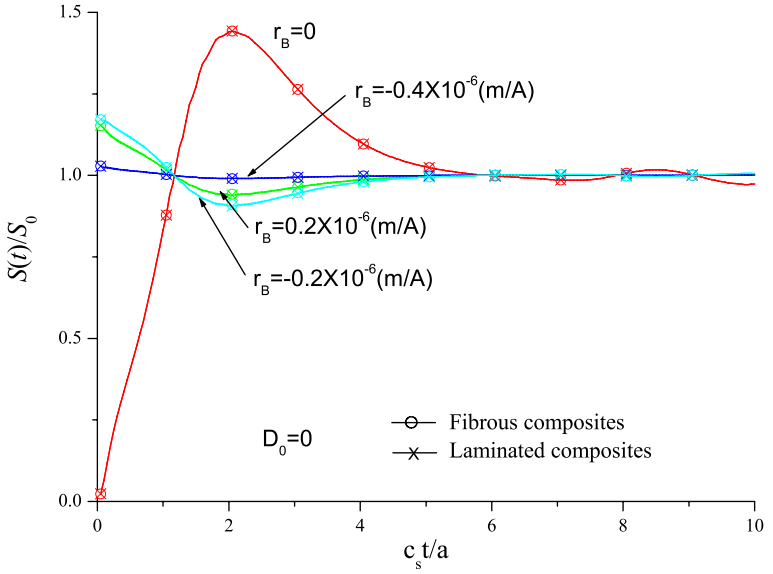

Fig. 12. Dynamic energy density factor vs normalized time for $D_0 = 0$.

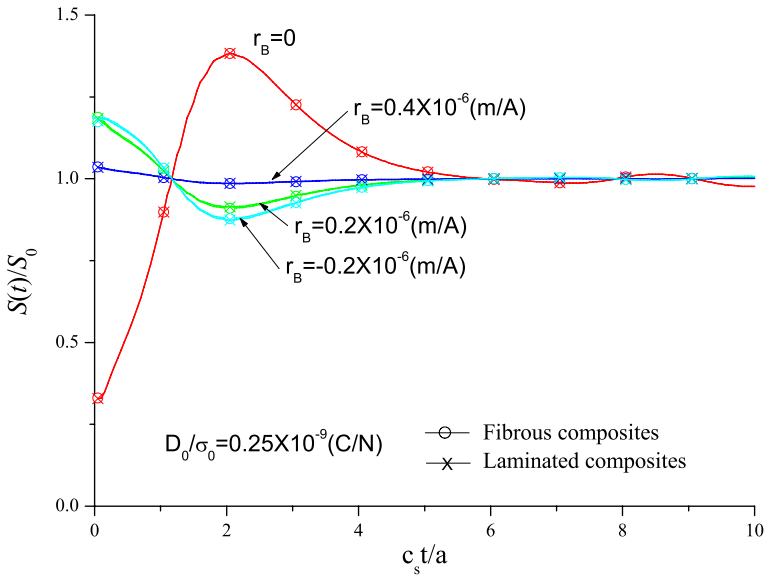

Fig. 13. Dynamic energy density factor vs normalized time for $D_0/\sigma_0 = 0.25 \times 10^{-9}$ C/N.

6. Conclusions

The dynamic problem involving a magnetoelectroelastic medium with a crack penetrating through the solid along the poling direction is analyzed under antiplane mechanical impact and inplane electric and magnetic impact loadings. The Fourier and Laplace transforms are employed to solve the associated mixed initial-boundary value problem. A Fredholm integral equation of the second kind is derived and solved via a numerical approach. Using a numerical inversion of the Laplace transform formulated by Stehfest, the dynamic intensity factors of COD and stress, and dynamic energy density factors are determined numerically in the time domain, and the numerical results are presented graphically to show the effects of the material properties and applied electric and magnetic impacts.

Acknowledgement

This work was supported by the National Natural Science Foundation of China under Grant No. 10272043. Some helpful suggestions for improving the original manuscript from one anonymous reviewer are greatly appreciated.

References

Aboudi, J., 2001. Micromechanical analysis of fully coupled electro-magneto-thermo-elastic multiphase composites. Smart Materials and Structures 10, 867–877.

Benveniste, Y., 1995. Magnetoelectric effect in fibrous composites with piezoelectric and piezomagnetic phases. Physics Review B 51, 16424–16427.

Chen, E.P., Sih, G.C., 1977. Elastodynamic Crack Problems. Noordhoff International Publishing, Leyden, The Netherland.

Davies, B., Martin, B., 1979. Numerical inversion of the Laplace transform: a survey and comparison of methods. Journal of Computational Physics 33, 1–32.

Fabrikant, V.I., 2003. Computation of infinite integrals involving three Bessel functions by introduction of new formalism. ZAMM 83, 363–374.

Gao, C.-F., Kessler, H., Balke, H., 2003a. Crack problems in magnetoelectroelastic solids. Part I: exact solution of a crack. International Journal of Engineering Science 41, 969–981.

Gao, C.-F., Kessler, H., Balke, H., 2003b. Crack problems in magnetoelectroelastic solids. Part II: general solutions of collinear cracks. International Journal of Engineering Science 41, 983–994.

Gao, C.-F., Tong, P., Zhang, T.-Y., 2003c. Interfacial crack problems in magneto-electroelastic solids. International Journal of Engineering Science 41, 2105–2121.

Huang, J.H., Chiu, Y.H., Liu, H.K., 1998. Magneto-electro-elastic Eshelby tensors for a piezoelectric–piezomagnetic composite reinforced by ellipsoidal inclusions. Journal of Applied Physics 83, 5364–5370.

Li, J.Y., 2000. Magnetoelectroelastic multi-inclusion and inhomogeneity problems and their applications in composite materials. International Journal of Engineering Science 38, 1993–2011.

Li, J.Y., Dunn, M.L., 1998. Micromechanics of magnetoelectroelastic composite materials: average field and effective behavior. Journal of Intelligent Materials Systems and Structures 9, 404–416.

Li, X.-F., Lee, K.Y., 2004a. Crack growth in a piezoelectric material with a Griffith crack perpendicular to the poling axis. Philosophical Magazine 84, 1789–1820.

Li, X.-F., Lee, K.Y., 2004b. Fracture analysis of cracked piezoelectric materials. International Journal of Solids and Structures 41, 4137–4161.

Liu, J.X., Liu, X.L., Zhao, Y.B., 2001. Green's functions for anisotropic magnetoelectro-elastic solids with an elliptical cavity or a crack. International Journal of Engineering Science 39, 1405–1418.

Miller, M.K., Guy, W.T., 1966. Numerical inversion of the Laplace transform of Jacobi polynomials. SIAM Journal of Numerical Analysis 3, 624–635.

Nan, C.W., 1994. Magnetoelectric effect in composites of piezoelectric and piezomagnetic phases. Physics Review B 50, 6082–6088.

Pak, Y.E., 1990. Crack extension force in a piezoelectric material. Journal of Applied Mechanics 57, 647–653.

Sih, G.C., Chen, E.P., 2003. Dilatational and distortional behavior of cracks in magnetoelectroelastic materials. Theoretical and Applied Fracture Mechanics 40, 1–21.

Sih, G.C., Jones, R., Song, Z.F., 2003. Piezomagnetic and piezoelectric poling effects on mode I and II crack initiation behavior of magnetoelectroelastic materials. Theoretical and Applied Fracture Mechanics 40, 161–186.

Sih, G.C., Song, Z.F., 2003. Magnetic and electric poling effects associated with crack growth in BaTiO3–CoFe2O4 composite. Theoretical and Applied Fracture Mechanics 39, 209–227.

Song, Z.F., Sih, G.C., 2003. Crack initiation behavior in magnetoelectroelastic composite under in-plane deformation. Theoretical and Applied Fracture Mechanics 39, 189–207.

Spyropoulos, C.P., Sih, G.C., Song, Z.F., 2003. Magnetoelectroelastic composite with poling parallel to plane of line crack under out-of-plane deformation. Theoretical and Applied Fracture Mechanics 39, 281–289.

Stehfest, H., 1970. Numerical inversion of Laplace transforms. Communications of ACM 13, 47–49, 624.

Wang, B.-L., Mai, Y.-W., 2004. Fracture of piezoelectromagnetic materials. Mechanics Research Communications 31, 65–73.

Wang, B.-L., Mai, Y.-W., 2003. Crack tip field in piezoelectric/piezomagnetic media. European Journal of Mechanics A/Solids 22, 591–602.

Wang, X., Shen, Y.P., 2002. The general solution of three-dimensional problems in magneto-electroelastic media. International Journal of Engineering Science 40, 1069–1080.

Wang, X., Zhong, Z., 2003. The general solution of spherically isotropic magnetoelectroelastic media and its applications. European Journal of Mechanics A/Solids 22, 953–969.